RESEARCH ARTICLE | APRIL 01 2024

Introducing dusty plasma particle growth of nanospherical titanium dioxide *⊗*

Special Collection: Plasma Sources for Advanced Semiconductor Applications

Bhavesh Ramkorun ⁽¹⁾; Swapneal Jain ⁽¹⁾; Adib Taba ⁽¹⁾; Masoud Mahjouri-Samani ⁽¹⁾; Michael E. Miller ⁽¹⁾; Saikat C. Thakur ⁽¹⁾; Edward Thomas, Jr. ⁽¹⁾; Ryan B. Comes ^{▼ (1)}



Appl. Phys. Lett. 124, 144102 (2024) https://doi.org/10.1063/5.0186797

A CHORUS





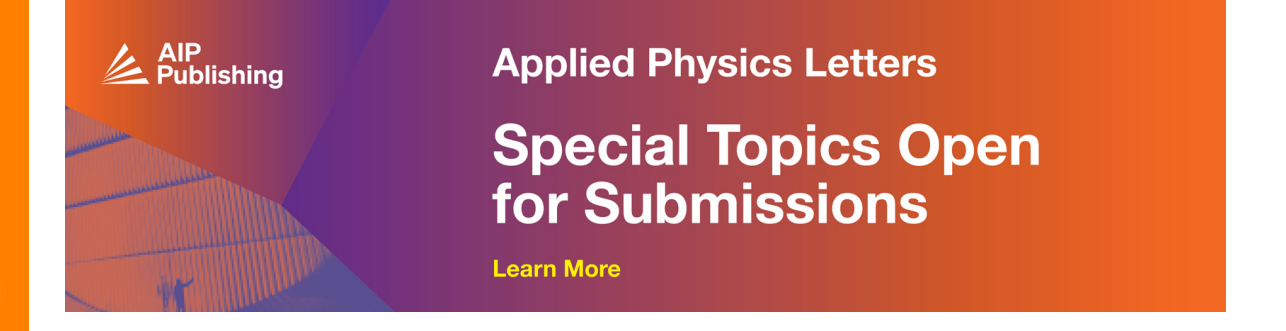
Articles You May Be Interested In

Effect of zinc precursor on morphology of ZnO nanoparticles

AIP Conf. Proc. (November 2020)

Vortex merging in strongly coupled dusty plasmas using a visco-elastic fluid model

Phys. Plasmas (May 2024)





Introducing dusty plasma particle growth of nanospherical titanium dioxide

Cite as: Appl. Phys. Lett. **124**, 144102 (2024); doi: 10.1063/5.0186797 Submitted: 8 November 2023 · Accepted: 22 March 2024 · Published Online: 1 April 2024







Bhavesh Ramkorun, no Swapneal Jain, no Adib Taba, no Masoud Mahjouri-Samani, no Michael E. Miller, no Saikat C. Thakur, no Edward Thomas, Jr., no and Ryan B. Comes no Saikat C. Thakur, no Edward Thomas, Jr., no and Ryan B. Comes no Saikat C. Thakur, no Saikat C

AFFILIATIONS

- Department of Physics, Auburn University, Auburn, Alabama 36849, USA
- ²Department of Electrical and Computer Engineering, Auburn University, Auburn, Alabama 36849, USA
- ³Auburn University Research Instrumentation Facility, Harrison College of Pharmacy, Auburn University, Auburn, Alabama 36849, USA

Note: This paper is part of the Special Topic: Plasma Sources for Advanced Semiconductor Applications.

a) Author to whom correspondence should be addressed: ryan.comes@auburn.edu

ABSTRACT

In dusty plasma environments, spontaneous growth of nanoparticles from reactive gases has been extensively studied for over three decades, primarily focusing on hydrocarbons and silicate particles. Here, we introduce the growth of titanium dioxide, a wide bandgap semiconductor, as dusty plasma nanoparticles. The resultant particles exhibited a spherical morphology and reached a maximum monodisperse radius of $235 \pm 20 \, \text{nm}$ after growing for $70 \, \text{s}$. The particle grew linearly, and the growth displayed a cyclic behavior; that is, upon reaching their maximum radius, the largest particles fell out of the plasma, and the next growth cycle immediately followed. The particles were collected after being grown for different amounts of time and imaged using scanning electron microscopy. Further characterization was carried out using energy dispersive x-ray spectroscopy, x-ray diffraction, and Raman spectroscopy to elucidate the chemical composition and crystalline properties of the maximally sized particles. Initially, the as-grown particles exhibited an amorphous structure after $70 \, \text{s}$. However, annealing treatments at temperatures of 400 and $800 \, ^{\circ}\text{C}$ induced crystallization, yielding anatase and rutile phases, respectively. Annealing at $600 \, ^{\circ}\text{C}$ resulted in a mixed phase of anatase and rutile. These findings open avenues for a rapid and controlled growth of titanium dioxide via dusty plasma.

Published under an exclusive license by AIP Publishing. https://doi.org/10.1063/5.0186797

A dusty plasma refers to a plasma, the fourth state of matter, that also contains solid particles ranging in size from nanometers to micrometers. These particles are commonly referred to as "dust." Extensive research has explored the spontaneous growth of particles from reactive gases in capacitively coupled plasmas (CCP), with a focus on generating either hydrocarbon or silicate dust, commonly from acetylene (C₂H₂) or silane (SiH₄) precursors, respectively.¹⁻⁷ In certain investigations, these particles have been collected and their detailed characterization was studied using techniques such as deuteron-beam-induced gamma-ray emission,² near-edge x-ray absorption fine structure spectroscopy (NEXAFS),³ and Raman spectroscopy.⁴ Furthermore, scanning electron microscopy (SEM)¹ and transmission electron microscopy (TEM)⁷ have consistently revealed that these particles exhibit spherical morphology, and their radii exhibited linear growth characteristics over time. Dusty plasma growth processes offer precise control over particles' size and morphology.8-1

These investigations have spurred the development of different particulates in dusty plasma systems, such as semiconductors and quantum dots. ^{13,14} Recently, organosilicon, conductive polymers, and metallic particles have been cultivated within CCP dusty plasma environments using hexamethyldisiloxane, ¹⁵ aniline, ¹⁶ and aluminum trichloride, ¹⁷ respectively. These precursors have traditionally found application in plasma-enhanced chemical vapor deposition (PECVD) for thin film production. ^{18–21}

This Letter introduces semiconducting titanium dioxide (TiO_2) particle growth within a dusty plasma environment. The growth process was initiated using titanium (IV) isopropoxide (TTIP) [$Ti(OC_3H_7)_4$] as the reactive precursor. X-ray diffraction (XRD) and Raman spectroscopy were employed to measure the crystal phases. SEM was used to image and subsequently measure the sizes of the particles grown as a function of time. SEM energy-dispersive x-ray spectroscopy (EDS) was used to ascertain the particles' chemical

composition. This investigation presents a dusty plasma growth technique for TiO_2 particles and introduces the material for further study in dusty plasmas.

The use of TTIP has had various applications for the production of $\rm TiO_2$ in both rutile and anatase polymorphs. A consistent observation in these investigations is the necessity of an annealing process to promote crystallization. In PECVD, thin films required annealing at temperatures exceeding 400 °C to crystallize. Thin films were also grown using atomic layer deposition. Although one study achieved anatase crystallization on substrates heated to 250 °C, another study annealed up to 900 °C to attain rutile crystallization. TTIP has also been employed in molecular beam epitaxy, in combination with an oxygen plasma, to grow rutile thin films on substrates heated to temperatures up to 725 °C. 26

Nucleation of nanoparticles and the formation of spherical aggregates are essential prerequisites for material growth. This phenomenon has been well-documented not only for ${\rm TiO_2}$ thin films 27,28 but also for various films containing carbon. $^{29-31}$ Dusty plasma has already exhibited rapid nucleation of nm-sized carbon particles within milliseconds, which can swiftly grow to hundreds of nanometers within seconds. 32,33 Here, we demonstrate that dusty plasma processes can

grow TiO_2 nanospheres within 10 s. These spheres continue to grow linearly until the end of a growth cycle. Although the as-grown particles collected after 70 s were initially amorphous, they crystallized into either anatase or rutile upon annealing at different temperatures. From the literature, rutile exhibits a direct wide bandgap and anatase exhibits an indirect wide bandgap.³⁴ They both have scientific applications as photocatalysts.³⁵

Figure 1(a) provides a schematic representation of the experimental setup with a plasma chamber housing 75 mm diameter electrodes spaced 25 mm apart. The top electrode had a powered region (50 mm), and the rest functioned as the grounded counter electrode. Electrode thicknesses were 13 mm (top) and 19 mm (bottom). A 1 mm slot in the bottom electrode held a 75 \times 25 mm² fused silica slide, serving as a substrate to collect nanoparticles. The chamber's base pressure was 3 \pm 0.3 mTorr. TTIP vapor entered the chamber up to a pressure of 35 \pm 3 mTorr, via a low flow metering valve and a gas line heated to 75 °C using a PID temperature controller. Argon (Ar) gas was then injected at 7 standard cubic centimeters per minute, which raised the chamber's pressure to 45 \pm 3 mTorr. The experimental pressure was then adjusted to 300 \pm 1 mTorr using an isolation valve connecting the chamber to the vacuum pump.

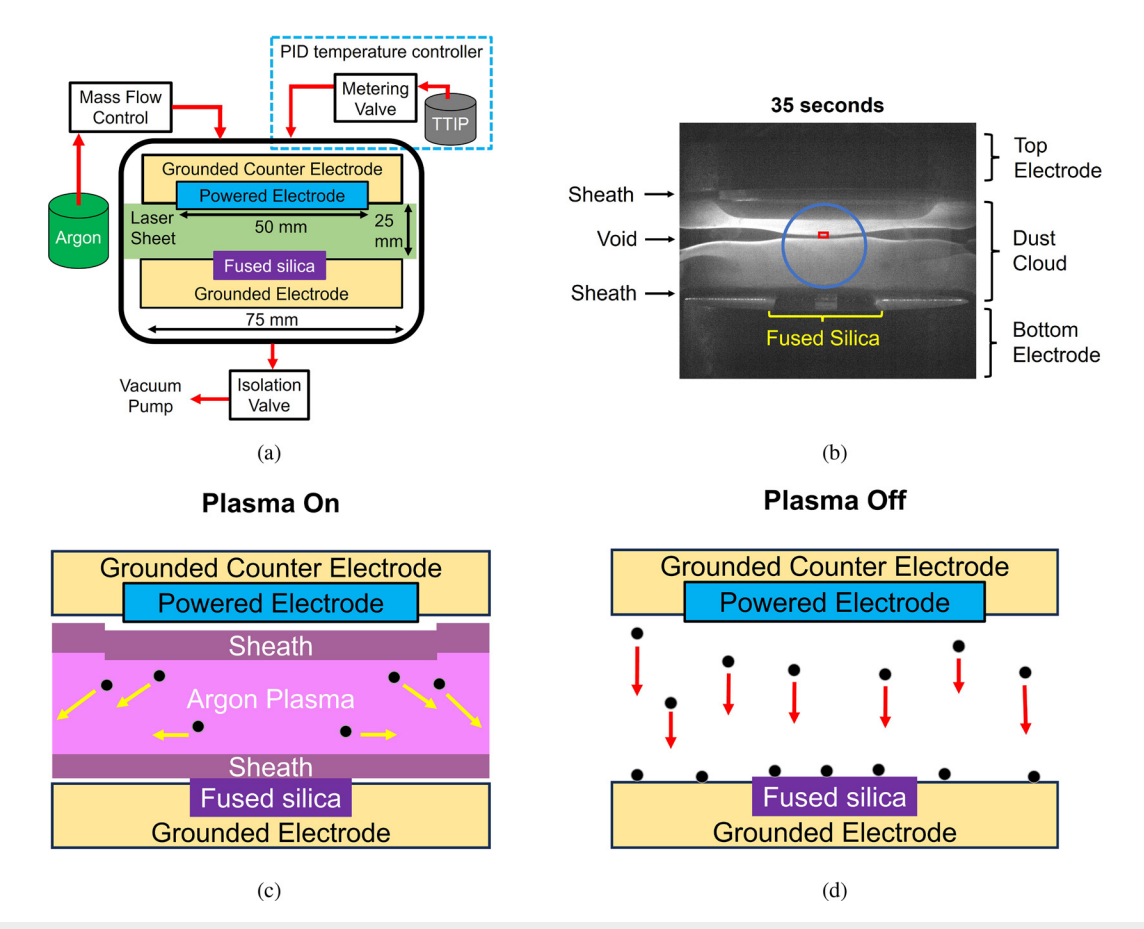


FIG. 1. (a) Schematic view of the experimental setup. (b) Photograph of dusty plasma at 35 s showing sheath, void, dust, electrodes, and fused silica. (c) Dust (black) transports (yellow arrow) out of the plasma at the end of a cycle with plasma energized. (d) Dust (black) deposits (red arrow) on the bottom electrode, including fused silica, when plasma is de-energized (schematics not to scale).

Throughout the paper, several terms will be used that are described here. *Energize* refers to the application of RF power to the top electrode for ionizing gases and igniting plasma. *De-energize* means the removal of RF power, causing the plasma to revert back to neutral gases. *Transport* occurs when the charged dust particles, having accumulated sufficient mass, leave the central plasma but are deflected by electric forces in the plasma to the sides of the experimental volume, as depicted in Fig. 1(c). *Deposition* occurs when the plasma is denergized, and dust particles experience gravitational and neutral drag forces, leading them to fall on the substrate, as depicted in Fig. 1(d).

The plasma was energized at 60 W during the initial 10 s and eventually at 30 W for the remainder of the experiments. This was to promote nucleation for 10 s, followed by continued growth at a reduced power. The dust particles formed a cloud, which was suspended between the electrodes by a balance of forces, including gravitational force, electric force due to the capacitively coupled electrodes, thermophoretic force, ion drag force, and neutral drag force. The magnitude of these forces depend on particle radius. This dependence is cubic for gravitational force and quadratic for the other forces. Gravitational force is negligible when the particles are nucleated in the first few seconds, but it gradually becomes the dominant force when the particles grow. The growth cycle ends when gravitational force overcomes the other forces, causing the particles to transport away from the central region of the plasma.

Three types of experiments were conducted to describe this dusty plasma. In *experiment A*, the upper electrode was energized for 260 s, leading to consecutive growth cycles of dusty plasma between the electrodes. The objective was to determine the cycle time of dust particle growth. In *experiment B*, the upper electrode was energized for a specific duration, and upon de-energization, dust particles deposited on the substrate. The objective was to gather particles at different times, analyze their radii, and establish correlations with the growth cycle. In *experiment C*, the upper electrode was energized for 70 s followed by a 45-s de-energization. The procedure was repeated 20 times, without breaking vacuum, to increase the density of dust particles collected for material characterization. During each plasma, the forward power was initially set to 60 W for 10 s, after which it was maintained at 30 W for the remaining 60 s.

In experiment A, a green laser sheet (532 nm) was directed into the plasma to visualize the dust cloud in two dimensions. A complementary metal oxide semiconductor (CMOS) camera recorded images of the cloud perpendicular to the laser sheet, up to a maximum of 50 frames per second. In Fig. 1(b), an image is shown. There was a recurrent appearance of a void, a dust-free region, in the central part of the plasma. This void exhibited cyclic expansion and contraction, mirroring the particle growth cycle. The laser light emission intensity of a region, highlighted in red was measured. This region covered some dust cloud and void in order to track the particle growth cycle. Concurrently, optical emission spectroscopy (OES) was employed to monitor the plasma, in the region highlighted in blue. A broadband spectrometer was utilized, boasting a resolution of 0.59 nm, a 25 micrometer slit size, a 600 lines/mm grating. Five data points, each with 100 ms integration time were averaged. The intensity of Ar I line at 763.5 nm, corresponding to the electric dipole transition of Ar from $3s^23p^5(^2P^0_{3/2})4p$ to $3s^23p^5(^2P^0_{3/2})4s$, was measured throughout the experiment. 39-41 The cyclic evolution of light emission and OES intensity were used to quantify the growth cycle. The resulting data, presented in Fig. 2, revealed that the growth cycle was approximately 77 ± 9 and 77 ± 4 s according to laser light and OES intensity, respectively. The phase difference between the two sets of data potentially arises from experimental differences between the two measurements. For example, OES has a bigger field of view than the region analyzed for laser light intensity. Furthermore, the cyclic variation in the two measurements is attributed to distinct physical mechanisms. The changes in the laser light intensity occur due to fluctuations in particle radii. Meanwhile, changes in the OES intensity occur due to changes in the population of excited Ar.

In experiment B, the plasma was energized for durations of either 10, 30, 50, 70, 90, 110, or 135 s to deposit nanoparticles on the substrate. SEM imaging was then employed to determine particle radii to correlate with the growth cycle, previously established as \sim 77 s in experiment A. Experiment B facilitated the analysis of particle radii from two cycles. When the plasma was energized and the growth cycle ended, particles were transported away from the plasma instead of depositing on the substrate. The sheath electric field deflected particles away from the electrodes and toward the plasma edges, as depicted in Fig. 1(c). Conversely, when the plasma was de-energized, the absence of the sheath electric field allowed particles to deposit on the bottom electrode and substrate, as depicted in Fig. 1(d). This enabled the collection and measurement of particle radii over time.

In Fig. 3(a), a linear progression in particles' radii from experiment B is observed as a function of plasma runtime. Subsequently, after a duration of \sim 77 s, the next cycle commenced. Particles from cycle 1 were still seen at 90 and 110 s, as shown in Fig. 3(b). Thus, two size distributions were collected. By 120 s, the first cycle's particles were entirely cleared from the plasma, as confirmed by CMOS camera analysis. Therefore, the radii at 135 s were monodisperse. The first 10 s was dominated by creation of radicals, ions, and species in the nucleation stage from the gas molecules. Because of the nonlinear dynamics

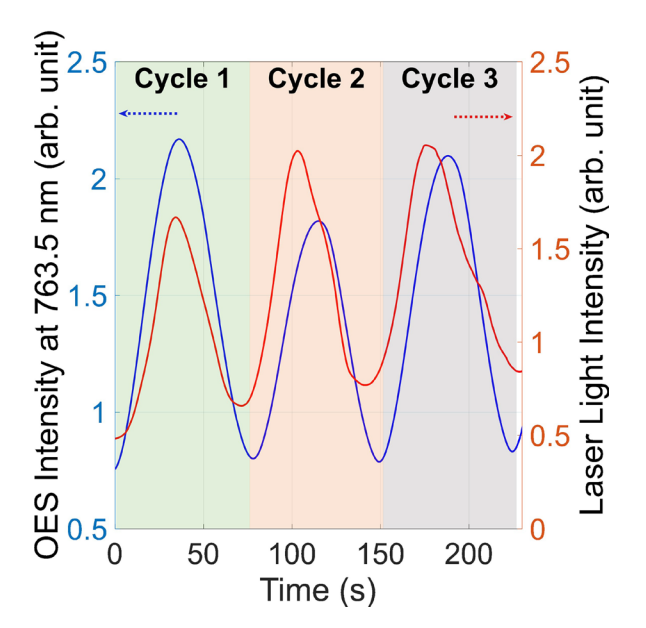
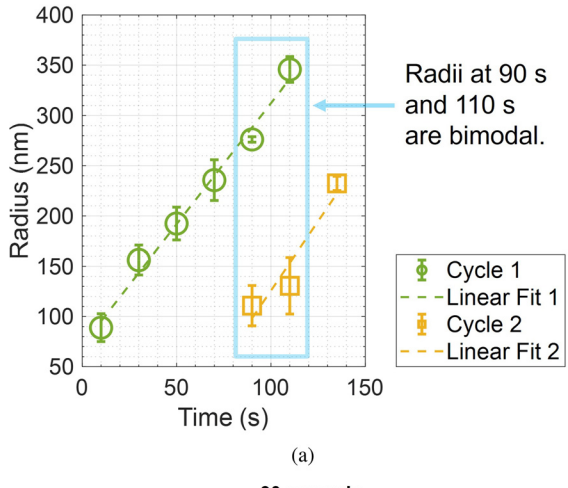


FIG. 2. OES at 763.5 nm and laser light intensity showing dusty plasma's cyclic behavior. Laser light intensity and OES intensity were measured from the red and blue region of Fig. 1(b), respectively, over three cycles.



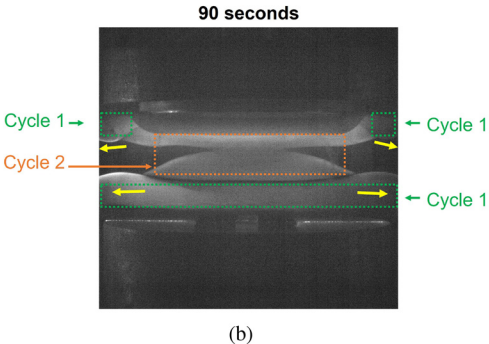
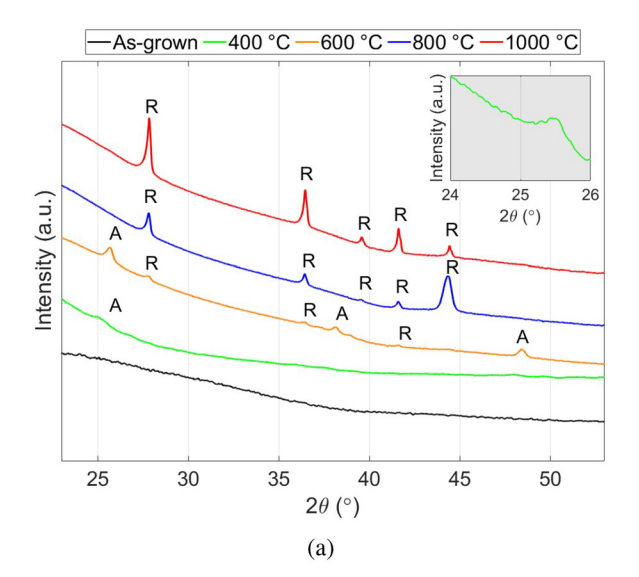


FIG. 3. (a) Particles' radii distribution over time, with linear fit applied to both cycles. At 90 and 110 s, bimodal radii distribution were observed, due to dust being present from two cycles. SEM image of the bimodal size distribution at 90 s is shown in Fig. 5(b). (b) Dust cloud at 90 s shows two cycles. Cycle 1 and 2 boxed in green and orange, respectively. Yellow arrows indicate dust from cycle 1 transporting away, similar to Fig. 1(c).

in this stage, we only considered the subsequent growth after $10\,\mathrm{s}$, whereby the linear growth was evident.

In experiment C, individual samples collected and annealed for two hours at either 400, 600, 800, or 1000 °C. XRD, as illustrated in Fig. 4(a), showed no peaks in the as-grown samples; hence they were amorphous. At 400 °C, TiO₂ crystallized into anatase, and at 800 °C, it crystallized into rutile. At 600 °C, a mixed phase of anatase and rutile was observed. XRD of the annealed samples confirmed that the particles matched the known powder diffraction pattern for each phase. The Raman spectra, as displayed in Fig. 4(b), closely resembled the known patterns for anatase and rutile. As mentioned earlier, annealing is generally required to crystallize TiO₂ grown from TTIP. However, when contrasted with the different aforementioned growth techniques, dusty plasma offers clear benefits, such as growing nanoparticles within just 10 s, providing precise control over size through a linear growth rate.

SEM images, illustrated in Fig. 5, were also used to calculate particles' radii before and after annealing. Monodisperse nanospheres were collected. These images clearly indicated a reduction in particles' radii following the annealing process. Particles that had been grown



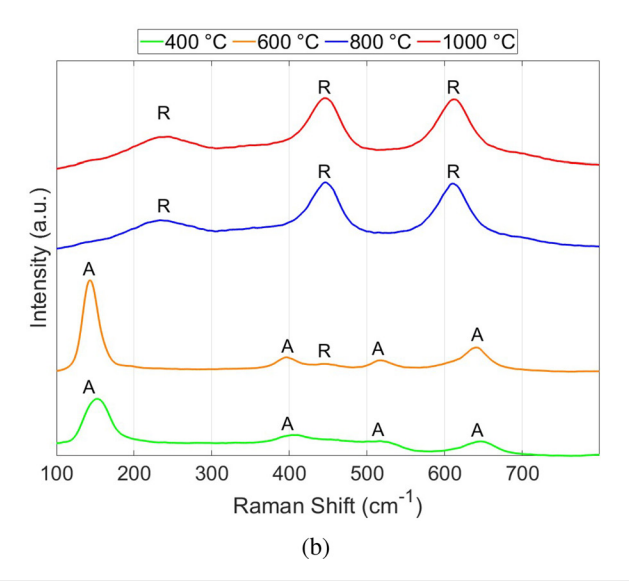


FIG. 4. Characterization of particles grown for 70 s with 2 h of annealing. (a) XRD, showing anatase (A) at 400 $^{\circ}$ C and rutile (R) at 800 and 1000 $^{\circ}$ C, with mixed phases at 600 $^{\circ}$ C. The inset show anatase XRD peak at 400 $^{\circ}$ C. (b) Raman spectroscopy.

for 70 s prior to annealing exhibited an average radius of 235 ± 20 nm, while particles subjected to a 2-h annealing treatment at 400 and 800 °C displayed a reduced average radius of 171 ± 12 and 134 ± 19 nm, respectively. SEM of a 90-s sample, with bimodal size distributions is also shown. Growing nanospheres via dusty plasma can potentially be compared to the Stober method of growth. The wet chemistry involved in the latter needs several hours to complete. Dusty plasma possibly offers a faster alternative.

Quantitative EDS analysis was performed on the samples. The findings, as summarized in Table I, showed a decline in the weight percentage of carbon (C) and an increase in titanium (Ti) and oxygen (O) on the samples after the annealing. The combined SEM and EDS

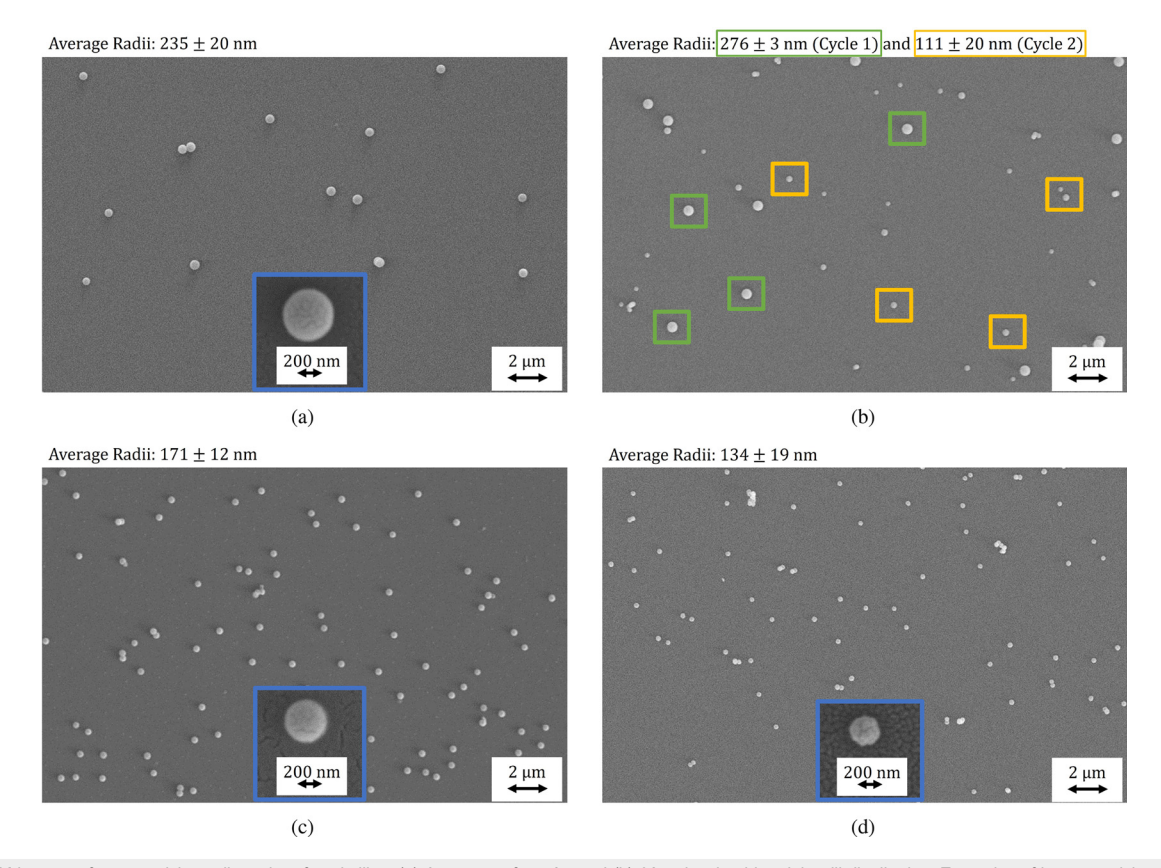


FIG. 5. SEM images of nanoparticles collected on fused silica. (a) As-grown after 70 s and (b) 90 s showing bimodal radii distribution. Examples of larger particles from cycle 1 and smaller particles from cycle 2 are boxed in green and yellow, respectively. After 70 s with (c) 400 °C anneal (anatase) and (d) 800 °C anneal (rutile).

results suggest that C was oxidized and desorbed from the nanoparticle during annealing, resulting in reduced C concentration and smaller particle radii. TTIP decomposed into molecules within the plasma, providing the source of Ti, O, and C in the nanoparticles. Fused silica substrates are the source of Si and additional O. In literature, PECVD experiments below $400\,^{\circ}\text{C}$ revealed TTIP dissociates into TiO₂, propene (C_3H_6) , and isopropanol (C_3H_8O) . The chemical pathway is elucidated in Eq. (1). A similar chemical pathway is possibly providing the source of the three aforementioned elements on the samples. Hydrogen has a low x-ray emission energy due to its low atomic number, making it difficult to detect via EDS. Future studies are needed to

 $\mbox{{\bf TABLE I.}}$ Impact of annealing on weight (%) of elements after 70 s growth, determined by EDS.

Element	Weight (%)				
	As-grown	400 °C	600 °C	800°C	1000 °C
СК	36.06	3.20	2.12	2.71	2.49
O K	26.43	42.32	48.60	44.37	50.34
Si K	31.32	39.07	28.18	34.79	15.23
Ti K	6.19	14.40	21.11	18.14	31.94

analyze the dissociation of TTIP *in situ*. For example, noninvasive methods like atomic mass spectrometry and Fourier transform infrared spectroscopy identified molecules and nucleation in previous studies, \$16,48-51

$$Ti(OC_3H_7)_4 \rightarrow TiO_2 + 2C_3H_6 + 2C_3H_8O.$$
 (1)

To explain the potential presence and oxidation of C from the surface of the nanodust, it is essential to delve into the three key stages of plasma particle growth: nucleation, coagulation, and agglomeration. 3,14,52-55 During nucleation, plasma species such as radicals and ions are generated through interactions between the background plasma and reactive gases. These species subsequently engage in chemical reactions, forming clusters with sizes \sim 1 nm. During coagulation, these clusters collide and bond, thus creating larger clusters with dimensions ~10 nm. Coagulation is dominated by chemisorption of ions and clusters. Nucleation and coagulation processes occur within the first few hundred milliseconds and seconds, respectively.³² The agglomeration stage, which can persist for several tens of seconds, involves the continued interaction of radicals and ions from the plasma, facilitating surface growth on the clusters and resulting in dust particles growing to several hundred nm. This is dominated by physisorption of ions and radicals on the clusters. MD simulation in the literature has shown that in Ar/SiH4 dusty plasma particle growth, the ratio of chemisorption to physisorption decreased with increasing

particle size.⁵⁶ Literature has also shown that smaller sized C₂H_x radicals exhibit longer lifetime than metallic radicals, during which their charge undergoes fluctuations, thereby causing surface growth on the dust through coulombic interactions.⁵⁷ This could potentially elucidate the presence of higher concentrations of Ti and O beneath certain layers of C, which subsequently undergo oxidation during the annealing process.

It is not a surprise that the bonding might have changed in the ${\rm TiO_2}$ nanoparticles between coagulation and agglomeration. A similar experiment was reported whereby NEXAFS was used to investigate the size-dependent chemical and physical properties of carbonaceous dust formed in a dusty plasma within a CCP system.³ The findings indicated that dust particles comprised an sp^2 -rich core with a 10 nm diameter, likely formed during coagulation, and an sp^2 -poor mantle with a diameter in the several hundred nm range, likely formed during agglomeration. It is plausible that a similar transformation in bonding may occur during the growth of ${\rm TiO_2}$ particles. There remain intriguing prospects for future research into the bonding characteristics of dusty ${\rm TiO_2}$ nanospheres. For example, further studies via TEM could examine the elemental distribution as a function of radius within the particles.

In this Letter, we have introduced a growth technique for TiO_2 via a TTIP metal-organic precursor that produces a dusty plasma. There was a growth cycle that lasted ~ 77 s, as measured by OES and CMOS camera images. Our experiments showed that TiO_2 particles can be grown to monodisperse sizes of 235 ± 20 nm within 70 s. SEM images revealed a linear growth rate in particles' radii over two growth cycles. Moreover, the samples after 70 s of the first cycle were collected 20 times and annealed to produce anatase and rutile phases. The results show room for future studies in particle growth using metal-organic precursors, characterization of particle chemistry and microstructure, and dusty plasma studies of interactions of particles with magnetic fields during growth.

The authors thank Tamara Isaacs-Smith and Cameron Royer for their assistance in conducting these experiments. We gratefully acknowledge the financial support received from the National Science Foundation EPSCoR program (OIA-2148653), U.S. Department of Energy—Plasma Science Facility (SC-0019176), and the NSF Major Research Instrumentation Grant (NSF-DMR-2018794), which made this work possible.

AUTHOR DECLARATIONS Conflict of Interest

The authors have no conflicts to disclose.

Author Contributions

Bhavesh Ramkorun: Conceptualization (equal); Formal analysis (lead); Investigation (lead); Methodology (lead); Visualization (lead); Writing – original draft (lead). Swapneal Jain: Investigation (supporting). Adib Taba: Investigation (supporting). Masoud Mahjouri-Samani: Resources (supporting); Supervision (supporting); Writing – review & editing (supporting). Michael Miller: Investigation (supporting); Resources (supporting). Saikat Chakraborty Thakur: Funding acquisition (supporting); Methodology (supporting); Project administration (supporting); Resources (supporting); Supervision (supporting); Writing – review & editing (equal). Edward Thomas Jr.: Funding acquisition (lead); Methodology (equal); Project administration

(equal); Resources (lead); Supervision (equal); Writing – review & editing (equal). **Ryan Comes:** Conceptualization (equal); Formal analysis (supporting); Methodology (equal); Project administration (equal); Resources (supporting); Supervision (equal); Writing – original draft (supporting); Writing – review & editing (equal).

DATA AVAILABILITY

The data that support the findings of this study are openly available in Auburn University Scholarly Repository at https://aurora.auburn.edu/handle/11200/50628?show=full, Ref. 58. Other data that support the findings of this study are available from the corresponding author upon request.

REFERENCES

- ¹E. Kovačević, I. Stefanović, J. Berndt, and J. Winter, "Infrared fingerprints and periodic formation of nanoparticles in Ar/C₂H₂ plasmas," J. Appl. Phys. **93**, 2924–2930 (2003).
- ²E. Kovačević, J. Berndt, I. Stefanović, H.-W. Becker, C. Godde, T. Strunskus, J. Winter, and L. Boufendi, "Formation and material analysis of plasma polymerized carbon nitride nanoparticles," J. Appl. Phys. 105, 104910 (2009).
- ³E. Kovacevic, J. Berndt, T. Strunskus, and L. Boufendi, "Size dependent characteristics of plasma synthesized carbonaceous nanoparticles," J. Appl. Phys. 112, 013303 (2012).
- ⁴L. Couëdel, D. Artis, M. P. Khanal, C. Pardanaud, S. Coussan, S. LeBlanc, T. Hall, E. Thomas, Jr., U. Konopka, M. Park, and C. Arnas, "Influence of magnetic field strength on nanoparticle growth in a capacitively-coupled radio-frequency Ar/C₂H₂ discharge," Plasma Res. Express 1, 015012 (2019).
- ⁵A. Bouchoule and L. Boufendi, "Particulate formation and dusty plasma behaviour in argon-silane RF discharge," Plasma Sources Sci. Technol. 2, 204 (1993).
 ⁶Y. Watanabe and M. Shiratani, "Growth kinetics and behavior of dust particles in silane plasmas," Jpn. J. Appl. Phys., Part 1 32, 3074 (1993).
- ⁷L. Boufendi and A. Bouchoule, "Particle nucleation and growth in a low-pressure argon-silane discharge," Plasma Sources Sci. Technol. 3, 262 (1994).
 ⁸B. Ganguly, A. Garscadden, J. Williams, and P. Haaland, "Growth and mor-
- ⁸B. Ganguly, A. Garscadden, J. Williams, and P. Haaland, "Growth and morphology of carbon grains," J. Vac. Sci. Technol., A 11, 1119–1125 (1993).
- ⁹A. Garscadden, B. Ganguly, P. Haaland, and J. Williams, "Overview of growth and behaviour of clusters and particles in plasmas," Plasma Sources Sci. Technol. 3, 239 (1994).
- ¹⁰J. Cao and T. Matsoukas, "Deposition kinetics on particles in a dusty plasma reactor," J. Appl. Phys. **92**, 2916–2922 (2002).
- ¹¹F. Galli and U. R. Kortshagen, "Charging, coagulation, and heating model of nanoparticles in a low-pressure plasma accounting for ion-neutral collisions," IEEE Trans. Plasma Sci. 38, 803–809 (2010).
- ¹²B. Chutia, T. Deka, Y. Bailung, S. Sharma, and H. Bailung, "A nanodusty plasma experiment to create extended dust clouds using reactive argon acetylene plasmas," Phys. Plasmas 28, 063703 (2021).
- ¹³U. Kortshagen, "Nonthermal plasma synthesis of semiconductor nanocrystals," J. Phys. D 42, 113001 (2009).
- ¹⁴L. Boufendi, M. Jouanny, E. Kovacevic, J. Berndt, and M. Mikikian, "Dusty plasma for nanotechnology," J. Phys. D 44, 174035 (2011).
- ¹⁵B. Despax, K. Makasheva, and H. Caquineau, "Cyclic powder formation during pulsed injection of hexamethyldisiloxane in an axially asymmetric radiofrequency argon discharge," J. Appl. Phys. 112, 093302 (2012).
- ¹⁶C. Pattyn, E. Kovacevic, S. Hussain, A. Dias, T. Lecas, and J. Berndt, "Nanoparticle formation in a low pressure argon/aniline RF plasma," Appl. Phys. Lett. 112, 013102 (2018).
- ¹⁷T. J. Cameron, B. Klause, H. P. Andaraarachchi, Z. Xiong, C. Reed, D. Thapa, C.-C. Wu, and U. R. Kortshagen, "Capacitively coupled nonthermal plasma synthesis of aluminum nanocrystals for enhanced yield and size control," Nanotechnology 34, 395601 (2023).
- ¹⁸H. Wang, C. Lin, and M. Hon, "The dependence of hardness on the density of amorphous alumina thin films by PECVD," Thin Solid Films 310, 260-264 (1997).

- ¹⁹T. Shirafuji, Y. Miyazaki, Y. Nakagami, Y. Hayashi, and S. Nishino, "Plasma copolymerization of tetrafluoroethylene/hexamethyldisiloxane and in situ Fourier transform infrared spectroscopy of its gas phase," Jpn. J. Appl. Phys., Part 1 38, 4520–4526 (1999).
- ²⁰Y. Shioya, H. Shimoda, K. Maeda, T. Ohdaira, R. Suzuki, and Y. Seino, "Low-k SiOCH film deposited by plasma-enhanced chemical vapor deposition using hexamethyldisiloxane and water vapor," Jpn. J. Appl. Phys., Part 1 44, 3879–3884 (2005).
- ²¹A. Airoudj, D. Debarnot, B. Bêche, and F. Poncin-Epaillard, "New sensitive layer based on pulsed plasma-polymerized aniline for integrated optical ammonia sensor," Anal. Chim. Acta 626, 44–52 (2008).
- ²²W. Lee, S. I. Woo, J. Kim, S. Choi, and K. Oh, "Preparation and properties of amorphous TiO₂ thin films by plasma enhanced chemical vapor deposition," Thin Solid Films 237, 105–111 (1994).
- ²³W. Yang and C. Wolden, "Plasma-enhanced chemical vapor deposition of TiO₂ thin films for dielectric applications," Thin Solid Films 515, 1708–1713 (2006).
- ²⁴J. Aarik, A. Aidla, T. Uustare, M. Ritala, and M. Leskelä, "Titanium isopropoxide as a precursor for atomic layer deposition: Characterization of titanium dioxide growth process," Appl. Surf. Sci. 161, 385–395 (2000).
- ²⁵J. Lee, S. J. Lee, W. B. Han, H. Jeon, J. Park, W. Jang, C. S. Yoon, and H. Jeon, "Deposition temperature dependence of titanium oxide thin films grown by remote-plasma atomic layer deposition," Phys. Status Solidi A 210, 276–284 (2013).
- ²⁶B. Jalan, R. Engel-Herbert, J. Cagnon, and S. Stemmer, "Growth modes in metal-organic molecular beam epitaxy of TiO₂ on *r*-plane sapphire," J. Vac. Sci. Technol., A 27, 230–233 (2009).
- ²⁷S. Huang and J.-S. Chen, "Comparison of the characteristics of TiO₂ films prepared by low-pressure and plasma-enhanced chemical vapor deposition," J. Mater. Sci.: Mater. Electron. 13, 77–81 (2002).
- ²⁸H. Nguyen, D. Kim, D. Park, and K. Kim, "Effect of initial precursor concentration on TiO₂ thin film nanostructures prepared by PCVD system," J. Energy Chem. 22, 375–381 (2013).
- ²⁹B. Stoner, G.-H. M. Ma, S. D. Wolter, and J. Glass, "Characterization of biasenhanced nucleation of diamond on silicon by *invacuo* surface analysis and transmission electron microscopy," Phys. Rev. B 45, 11067 (1992).
- 30 M. Kuhr, S. Reinke, and W. Kulisch, "Nucleation of cubic boron nitride (c-BN) with ion-induced plasma-enhanced CVD," Diamond Relat. Mater. 4, 375–380 (1995)
- ⁵¹B. Ramkorun, K. Chakrabarty, and S. Catledge, "Effects of direct current bias on nucleation density of superhard boron-rich boron carbide films made by microwave plasma chemical vapor deposition," Mater. Res. Express 8, 046401 (2021).
- $^{\bf 32} L.$ Ravi and S. Girshick, "Coagulation of nanoparticles in a plasma," Phys. Rev. E 79, 026408 (2009).
- ³³S. Groth, F. Greiner, B. Tadsen, and A. Piel, "Kinetic Mie ellipsometry to determine the time-resolved particle growth in nanodusty plasmas," J. Phys. D 48, 465203 (2015).
- ³⁴J. Zhang, P. Zhou, J. Liu, and J. Yu, "New understanding of the difference of photocatalytic activity among anatase, rutile and brookite TiO₂," Phys. Chem. Chem. Phys. 16, 20382–20386 (2014).
- 35T. Luttrell, S. Halpegamage, J. Tao, A. Kramer, E. Sutter, and M. Batzill, "Why is anatase a better photocatalyst than rutile?—Model studies on epitaxial TiO₂ films," Sci. Rep. 4, 4043 (2014).
- 36 J. Berndt, S. Hong, E. Kovačević, I. Stefanović, and J. Winter, "Dust particle formation in low pressure Ar/CH₄ and Ar/C₂H₂ discharges used for thin film deposition," Vacuum 71, 377–390 (2003).
- ³⁷R. Merlino, Dusty Plasmas and Applications in Space and Industry (Transworld Research Network Kerala, India, 2006), Vol. 81, pp. 73–110.
- ³⁸F. V. de Wetering, R. Brooimans, S. Nijdam, J. Beckers, and G. Kroesen, "Fast and interrupted expansion in cyclic void growth in dusty plasma," J. Phys. D 48, 035204 (2015).

- 39G. Norlén, "Wavelengths and energy levels of Ar I and Ar II based on new interferometric measurements in the Region 3 400-9 800 Å," Phys. Scr. 8, 249 (1973).
- 40W. Wiese, J. Brault, K. Danzmann, V. Helbig, and M. Kock, "Unified set of atomic transition probabilities for neutral argon," Phys. Rev. A 39, 2461 (1989).
- ⁴¹A. Kramida, Yu. Ralchenko, J. Reader, and NIST ASD Team, NIST Atomic Spectra Database (ver. 5.10) (National Institute of Standards and Technology, Gaithersburg, MD, 2022).
- ⁴²U. Balachandran and N. Eror, "Raman spectra of titanium dioxide," J. Solid State Chem. 42, 276–282 (1982).
- ⁴³W. Stöber, A. Fink, and E. Bohn, "Controlled growth of monodisperse silica spheres in the micron size range," J. Colloid Interface Sci. 26, 62–69 (1968).
- 44 J. Liu, S. Z. Qiao, H. Liu, J. Chen, A. Orpe, D. Zhao, and G. Q. Lu, "Extension of the Stöber method to the preparation of monodisperse resorcinol-formaldehyde resin polymer and carbon spheres," Angew. Chem. 123, 6069–6073 (2011).
- 45Y. Wang, H. Yang, and W. Zou, "Preparation of amorphous sphere-like TiO₂ with excellent photocatalytic performance," Mater. Lett. 254, 54–57 (2019).
- ⁴⁶C. P. Fictorie, J. F. Evans, and W. L. Gladfelter, "Kinetic and mechanistic study of the chemical vapor deposition of titanium dioxide thin films using tetrakis-(isopropoxo)-titanium (IV)," J. Vac. Sci. Technol., A 12, 1108–1113 (1994).
- ⁴⁷K.-H. Ahn, Y.-B. Park, and D.-W. Park, "Kinetic and mechanistic study on the chemical vapor deposition of titanium dioxide thin films by in situ FT-IR using TTIP," Surf. Coat. Technol. 171, 198–204 (2003).
- ⁴⁸G. Kroesen, J. Den Boer, L. Boufendi, F. Vivet, M. Khouli, A. Bouchoule, and F. De Hoog, "In situ infrared absorption spectroscopy of dusty plasmas," J. Vac. Sci. Technol., A 14, 546–549 (1996).
- ⁴⁹C. Deschenaux, A. Affolter, D. Magni, C. Hollenstein, and P. Fayet, "Investigations of CH₄, C₂H₂ and C₂H₄ dusty rf plasmas by means of FTIR absorption spectroscopy and mass spectrometry," J. Phys. D 32, 1876 (1999).
- 50K. Ouaras, L. C. Delacqua, G. Lombardi, J. Röpcke, M. Wartel, X. Bonnin, M. Redolfi, and K. Hassouni, "In-situ diagnostics of hydrocarbon dusty plasmas using quantum cascade laser absorption spectroscopy and mass spectrometry," J. Plasma Phys. 80, 833–841 (2014).
- ⁵¹I. Denysenko, E. von Wahl, S. Labidi, M. Mikikian, H. Kersten, T. Gibert, E. Kovačević, and N. A. Azarenkov, "Modeling of argon–acetylene dusty plasma," Plasma Phys. Controlled Fusion 61, 014014 (2018).
- 52I. Stefanovic, E. Kovacevic, J. Berndt, and J. Winter, "Hα emission in the presence of dust in an Ar-C₂H₂ radio-frequency discharge," New J. Phys. 5, 39 (2003).
- ⁵³T. Donders, T. Staps, and J. Beckers, "Characterization of cyclic dust growth in a low-pressure, radio-frequency driven argon-hexamethyldisiloxane plasma," J. Phys. D 55, 395203 (2022).
- ⁵⁴A. Fridman, L. Boufendi, T. Hbid, B. Potapkin, and A. Bouchoule, "Dusty plasma formation: Physics and critical phenomena. Theoretical approach," J. Appl. Phys. **79**, 1303–1314 (1996).
- 55B. Ramkorun, G. Chandrasekhar, V. Rangari, S. C. Thakur, R. B. Comes, and E. Thomas, Jr., "Comparing growth of titania and carbonaceous dusty nanoparticles in weakly magnetised capacitively coupled plasmas," arXiv:2402.00951 (2024).
- ⁵⁶X. Shi, P. Elvati, and A. Violi, "On the growth of Si nanoparticles in non-thermal plasma: Physisorption to chemisorption conversion," J. Phys. D 54, 365203 (2021).
- ⁵⁷J. Winter, "Dust in fusion devices—A multi-faceted problem connecting highand low-temperature plasma physics," Plasma Phys. Controlled Fusion 46, B583 (2004).
- 58B. Ramkorun (2023). "Ar/TTIP dust cloud," Auburn University. http://dx.doi.org/ 10.35099/aurora-696